Molecular Orientation at Rubbed Polyimide Surfaces Determined with X-ray Absorption Spectroscopy: Relevance for Liquid Crystal Alignment

Klaus Weiss,[†] Christof Wöll,[†] Edgar Böhm,[‡] Bernd Fiebranz,[‡] Gerd Forstmann,[§] Bin Peng,[§,||] Volker Scheumann,[§] and Diethelm Johannsmann*[,§]

Physical Chemistry I, University of Bochum, 44780 Bochum, Germany, Merck KGaA, Frankfurter Strasse 250, 64371 Darmstadt, Germany, and Max-Planck-Institute of Polymer Research, P.O. Box 3148, 55021 Mainz, Germany

Received July 17, 1997; Revised Manuscript Received January 5, 1998

ABSTRACT: The molecular orientation at the surface of polyimide (PI) alignment layers used for liquid crystal displays has been determined using X-ray absorption spectroscopy (NEXAFS). The second moments of the orientation distribution function obtained from a detailed analysis reveal that, upon rubbing, the PI substrates develop biaxiality and an inclination of a few degrees. For a nematic liquid crystal (LC) in contact with these alignment layers, the pretilt angle was determined and revealed a weak correlation with buffing strength.

Introduction

The alignment of liquid crystals (LCs) via an anisotropic interaction with the cell surface ("orientational surface anchoring"[1−4]) has recently gained considerable attention due to its practical importance in liquid crystal display (LCD) technology[5] and because of the fundamental interest in understanding and separating the various forces acting on the nematic material close to the solid−LC interface. Although some general trends have been well established in practice,[6] a detailed understanding of the underlying microscopic mechanisms, by which orientational and positional order in the LC film is created through LC−polymer surface interactions (dipolar, electrostatic, van der Waals, entropic, ...), is lacking for the most part. Of particular interest is the "pretilt angle", which gives the inclination of the LC nematic axis away from the surface (see Figure 1).[7] In most practical applications, such as the twisted nematic (TN) and the supertwisted nematic (STN) LC cells, a sufficiently large pretilt angle is needed to avoid inversion lines. Not only are high pretilt angles difficult to achieve, but also the prediction of a pretilt angle for a given combination of alignment layer and liquid crystal is presently impossible.

Although a couple of different schemes for inducing LC alignment from the cell surface are under discussion,[8−10] the rubbing technique is the dominating approach today. Here, an in-plane anisotropy is generated by rubbing polyimide surfaces with a cloth. Typically, there is a pretilt angle of 1−10° directed along the buffing direction. IR-birefringence studies have demonstrated the existence of chain elongation in the buffed layers along the buffing direction.[11] Sakamato and co-workers have carried out a detailed study on PMDA−ODA polyimide films (for the chemical structure see below) of varying thickness and found that the principal axes of anisotropy were inclined with respect to the sample surface by 8°.[12] Studies using X-ray diffraction[13,14] have shown that near surface crystallinity is of importance. Presumably, the polar in-plane anisotropy is connected to microcrystallites with certain preferred crystallographic axes exposed at the surface.

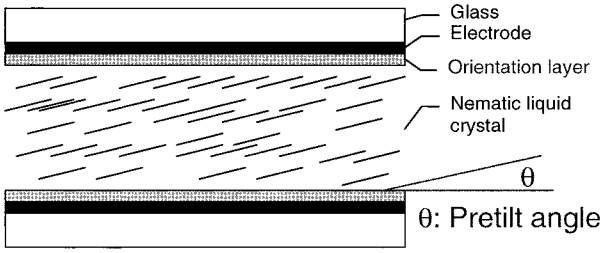

Figure 1. Schematic of a liquid crystal cell without twist. A pretilt tilt angle is a critical requirement for liquid crystal displays.

Because the physics of the solid−LC interface can be potentially very complicated, there is great need for experimental techniques to study the molecular order close to the interface in more detail. Shen and coworkers have used surface optical second harmonic generation (SHG) to investigate the orientational distribution function (ODF) of LC monolayers on various polymer surfaces and found that it depends on the chemical and structural properties of the surface as well as the buffing procedure.[15−19] A semiquantitative model has been developed to connect certain moments of the LC surface orientational distribution to the LC bulk pretilt angles.[16] A second important step is to make the connection between the orientational order of the LC surface layer and the structure of the polymer surface. In contrast to the first LC layer, the polyimide substrate is not accessible to the optical second harmonic generation because the molecules have inversion symmetry. We have therefore used "near-edge X-ray absorption fine structure" (NEXAFS) spectroscopy. In the past, NEXAFS has been mainly used to study the molecular orientation in thin organic layers,[20−23] but recently, the technique has also been successfully applied to neat and modified polymer surfaces.[24,25] Monitoring the X-ray absorption by recording the secondary electron yield results in a pronounced surface sensitivity due to the small escape depth of the secondary electrons (about 2 nm for the present experiments).

* Author for correspondence.
[†] University of Bochum.
[‡] Merck KGaA.
§Max-Planck-Institute of Polymer Research.
[||] On leave from Department of Chemical Technology, Huadong University, Zhanjiang City, Guandong Province, 424064 Peoples Republic of China.

S0024-9297(97)01075-9 CCC: $15.00
Published on Web 02/28/1998

Note that, in case of NEXAFS, local field problems[26] do not arise because of the small polarizabilities encountered in the soft X-ray domain. This is a prominent advantage compared to optical SHG[15−18] or IR-birefringence.[12]

In previous NEXAFS experiments, Ouchi and coworkers have compared the surface orientation of two different homologous series of polyimides.[27,28] They found that the angular position of the X-ray absorption minimum deviated from normal incidence by several degrees. They derived a molecular picture of the near surface polymer conformation that correlates with the results of surface SHG and bulk tilt angle measurements. Stöhr and co-workers have investigated the orientation of near-surface layers of polyimide under conditions of varying buffing strength with NEXAFS.[29] They found an alignment depth of about 100 Å. The amount of buffing-induced tilt was not addressed in this study.

Here, we provide the results of a complete analysis of NEXAFS data, yielding the full tensorial information on the second moments of polyimide segment orientations at various buffing strengths. The results are compared to the pretilt angle in an LC cell in contact with the buffed PI surfaces as obtained from measurements using a crystal rotation setup.

Theory

Most systems studied so far with NEXAFS exhibited a high symmetry with regard to the surface normal (3-fold or higher rotation axis), resulting in the absence of any azimuthal dependence of resonance intensities. In the present case, the number of symmetry elements is effectively reduced to a mirror plane containing the surface normal and the buffing direction (C_s symmetry), and the analysis appropriate for a C_{2v} symmetry[30] cannot be applied. Therefore, in the following we will briefly outline the analysis procedure. For aromatic systems the transition dipole moments of the C1s $\rightarrow \pi^*$ transition are oriented perpendicular to the ring planes and the linear dichroism observed for the excitation probabilities as a function of photon angle of incidence θ is generally given by a second-order trigonometric function, $a + b\cos(2(\theta - \theta_0))$. θ_0 is the substrate pretilt. The ratio b/a is an indicator of the amount of anisotropy, for isotropic surfaces we have $b = 0$. Angular scans along and perpendicular to the buffing direction can provide the full second rank tensor of second moments of the orientational distribution function $\underline{Q}$. The X-ray absorption $A(\hat{p})$ as a function of the electric field vector $\hat{p}$ can be written as

$$\begin{aligned} A(\hat{p}) &= 3\bar{A}\langle(\hat{p}\cdot\hat{n})^2\rangle \\ &= \bar{A}\sum_{i,j=1}^{3}\hat{p}_i\hat{p}_j\langle\hat{n}_i\hat{n}_j\rangle \\ &= 3\bar{A}\hat{p}\cdot\underline{\underline{K}}\cdot\hat{p} \end{aligned} \tag{1}$$

The hat denotes a unit vector. Angular brackets $\langle\ \rangle$ denote the orientational average $\langle a\rangle = \int a(\theta_m,\varphi_m)\, f(\theta_m,\varphi_m) \sin\theta_m\, d\varphi_m\, d\theta_m$ with $f(\theta_m,\varphi_m)$ the orientational distribution function (ODF). n is the direction of a given transition dipole moment, and θ_m and φ_m are the corresponding polar and azimuthal angles. $\bar{A}$ is the X-ray absorption averaged over all directions of **E** vectors. $\underline{\underline{K}} = \langle n_i n_j\rangle$ is the matrix of orientation factors.[31]

To focus on anisotropies, we consider the Saupe matrix

$$\underline{\underline{Q}} = \frac{3\underline{\underline{K}} - \underline{\underline{I}}}{2} \tag{2}$$

where $\underline{\underline{I}}$ is the identity matrix. $\underline{\underline{Q}}$ has been constructed to serve as a convenient order parameter for media with quadrupolar symmetry. In nematic liquid crystals the Saupe matrix is known as the tensorial order parameter.[32] For an isotropic medium $\underline{\underline{Q}}$ is identical to zero. For perfect alignment along the z-direction Q_{zz} is 1. Because the trace of $\underline{\underline{Q}}$ is zero, $\underline{\underline{Q}}$ does not depend on the density of the medium. In terms of the Saupe matrix, eq 1 reads

$$\frac{A(\hat{p}) - \bar{A}}{2\bar{A}} = \hat{p}\cdot\underline{\underline{Q}}\cdot\hat{p} \tag{3}$$

Since $\underline{\underline{Q}}$ is symmetric, it can be diagonalized to

$$\underline{\underline{Q}}^{\mathrm{dia}} = \begin{bmatrix} -(S+P)/2 & 0 & 0 \\ 0 & -(S-P)/2 & 0 \\ 0 & 0 & S \end{bmatrix} \tag{4}$$

where S is the uniaxial order parameter known from nematic liquid crystals and P is the biaxiality. For nematic liquid crystals the biaxiality vanishes in the bulk ($P = 0$). The use of the term biaxiality does by no means imply a biaxialty of the average main chain conformation such as obtained for polymer foils that have been stretched in two different directions. We only discuss the biaxial symmetry of the aromatic units. In the following, we show how the order parameters S and P as well as the angle of rotation rendering the Saupe matrix diagonal θ_0 can be derived from the measurement of X-ray dichroism. Some details of the mathematics have been referred to in the Appendix.

The definition of S and P in the diagonal matrix implies a choice of a primary axis. For uniaxial systems one usually picks the symmetry axis. For biaxial systems the axis with the highest diagonal component of the Saupe matrix is chosen. For the present analysis the z-axis was used as the primary axis. It is a symmetry axis for untreated samples. Upon buffing, a biaxiality is generated. The transition dipole moments $\hat{n}$ for the transitions seen in NEXAFS are oriented perpendicular to the main chain subunits and, as a result, the corresponding order parameter S only indirectly describes the main chain orientation. When discussing the Saupe tensor of LC monolayers adsorbed to an alignment layer, the primary axis should be chosen as the LC molecules' main axis, which is again perpendicular to C1s$-\pi^*$ transition dipole moments.

The Saupe matrix is specified by the quantities S, P, and the three Euler angles of rotation rendering $\underline{\underline{Q}}$ diagonal. In the given experimental situation, two of the three Euler angles are zero by symmetry. The point symmetry group of a buffed polyimide surface is C_s with a mirror plane spanned by the surface normal and the buffing direction. Diagonalization is achieved by rotating the coordinate system around the y-axis by an angle θ_0. The maximum information to be extracted from NEXAFS spectra is the set of numbers S, P, and θ_0.

The **Q** tensor is determined experimentally by varying the orientation of the sample with respect to the **E** vector of the soft X-ray photons. Two different types of angular scans are recorded. In the first case (termed

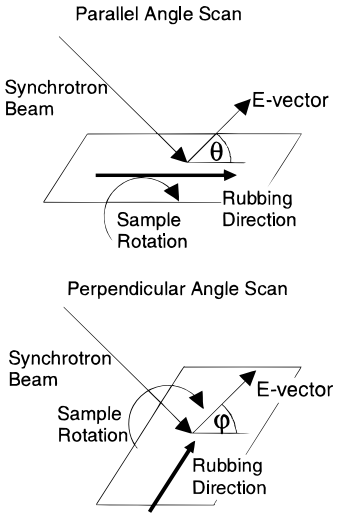

Figure 2. Geometry of the experiment. "Parallel" scans probe the anisotropy in the plane given by the surface normal and the buffing direction, while "perpendicular" scans probe the anisotropy perpendicular to it.

"parallel"), the **E** vector is rotated around an axis normal to both the buffing direction and the surface normal between $\theta = 0°$ (**E** vector parallel to the sample surface) and $\theta = \pm 60°$. In the second type of scan (termed "perpendicular"), the **E** vector is rotated around the buffing direction between $\varphi = 0$ (**E** vector in the sample surface) and $\varphi = \pm 60°$. Figure 2 depicts the geometry.

To derive S, P, and θ_0 from the angle dependence of NEXAFS intensities, eq 3 has to be expressed in laboratory coordinates. We find

$$\frac{A(\theta)}{\bar{A}} = \frac{2 + S - P}{2} - \frac{3S + P}{2}\cos(2(\theta - \theta_0)) \quad (5a)$$

$$\frac{A(\varphi)}{\bar{A}} = \frac{4 - S + P + (P + 3S)\cos(2\theta_0)}{4} + \frac{3(P - S) - (P + 3S)\cos(2\theta_0)}{4}\cos(2\varphi) \quad (5b)$$

for the parallel and the perpendicular scans, respectively. From fitting the functions $A(\theta) = a_\theta + b_\theta \cos(2(\theta - \theta_0))$ and $A(\varphi) = a_\varphi + b_\varphi \cos(2\varphi)$ to the experimentally determined NEXAFS intensities, we can thus determine θ_0 directly from the parallel scan. Additionally, we obtain b_0 and a_0, which are connected to P and S by

$$\frac{b_\theta}{a_\theta} = \frac{P + 3S}{P - S - 2} \quad (6a)$$

$$\frac{b_\varphi}{a_\varphi} = \frac{3(P - S) - (P + 3S)\cos(2\theta_0)}{4 + P - S + (P + 3S)\cos(2\theta_0)} \quad (6b)$$

The inversion of eqs 6 with respect to S and P gives

$$S = -\frac{1}{2}\frac{3\alpha(\beta - 1) - 2\beta + \alpha(\beta + 1)\cos(2\theta_0)}{\beta - 3 + \alpha(\beta + 1)\cos(2\theta_0)} \quad (7a)$$

$$P = \frac{3}{2}\frac{-\alpha(\beta - 1) - 2\beta + \alpha(\beta + 1)\cos(2\theta_0)}{\beta - 3 + \alpha(\beta + 1)\cos(2\theta_0)} \quad (7b)$$

where $\alpha = b_\theta/a_\theta$ and $\beta = b_\varphi/a_\varphi$. If the angle θ_0 is small,

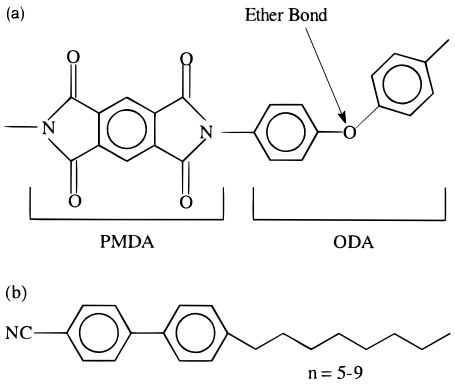

Figure 3. (a) Chemical structure of poly(pyromellitimidooxydianiline) (PMDA−ODA polyimide). (b) Chemical structure of the liquid crystal E7.

this relation can be approximated by

$$S \approx \frac{\alpha + \beta - 2\alpha\beta}{\alpha + \beta + \alpha\beta - 3} \quad (8a)$$

$$P \approx \frac{3(\alpha - \beta)}{\alpha + \beta + \alpha\beta - 3} \quad (8b)$$

For the data discussed below eqs 7 and 8 yield very similar order parameters. Finally, for untreated surfaces, we expect $\theta_0 = 0$ and $\alpha = \beta$ which result in

$$S \approx \frac{2\alpha(1 - \alpha)}{2\alpha + \alpha^2 - 3} \quad (9a)$$

$$P \approx 0 \quad (9b)$$

From fitting eqs 5 to angle dependent NEXAFS intensities, as shown in Figure 5, we can derive the parameters S, P, and θ_0 for the PMDA and the ODA units for the different buffing strengths.

Experimental Section

For the present experiments (PMDA−ODA) polyimide (poly(pyromellitimidooxydianiline) was used. Although this material is not specifically optimized for LC alignment, it is widely used for that purpose when the technical demands are not severe. Figure 3a shows the chemical structure. The ether bond is the only flexible link in the structure. Between two ether bonds, the structure is rigid. In the bulk there is a certain degree of crystallinity with mostly flat zigzag packing.[33,34] Takahashi et al. have found smectic liquid crystalline ordering under some conditions.[35] Factor et al. have studied the near surface order of (unrubbed) PMDA−ODA polyimide with grazing incidence X-ray diffraction (GIXS).[36,37] They found an increased crystallinity close to the film−air interface. The zigzag conformation is more planar at the interface than in the bulk, as evidence by an increased d spacing along the chain. Also, the order perpendicular the chains increases.

The polymer was printed onto silicon wafers using an adhesion promoter (VM-651 from DuPont). Buffing was performed with a Yoshikawa YA-20-R cloth. Three buffing strengths termed "weak", "normal", and "strong" as well as an untreated sample were investigated. The buffing distance, which is the integrated length of cloth in contact with any given spot on the sample was 53, 105, and 193 cm. The pile impression was 0.1, 0.4, and 0.6 mm.

The bulk pretilt angles of the liquid crystal in contact with the different substrates studied here were measured with a conventional crystal rotation setup.[38,39] The liquid crystal employed was E7 from Merck, a mixture of various cyanobiphenyls. Figure 3b shows the chemical structure.

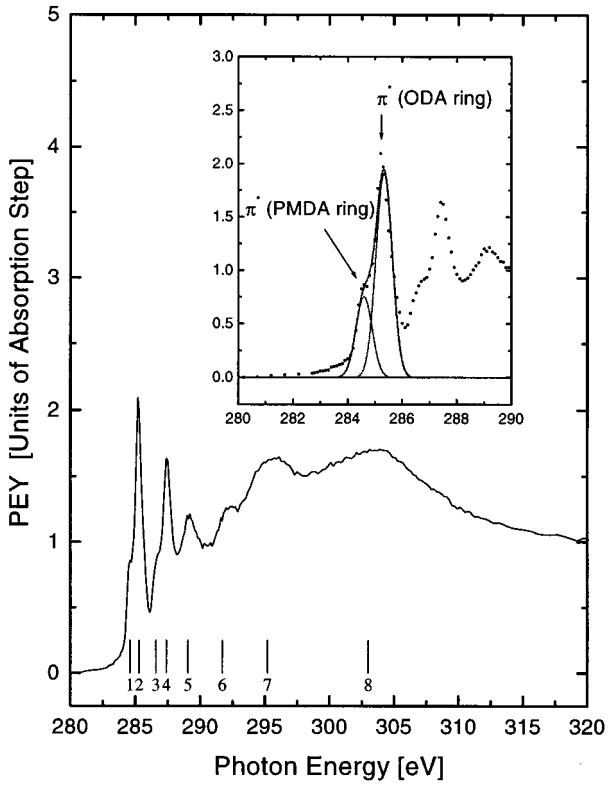

Figure 4. Typical NEXAFS spectrum (partial electron yield, PEY) for normally buffed PMDA−ODA. The resonances are labeled by integer numbers. The peak assignments are given in Table 1.

The NEXAFS measurements were performed at beamline HE-PGM3 of the synchrotron radiation facility BESSY (Berlin, Germany) using the experimental station HIRES. The spectra were recorded at the C1s absorption edge with an energy resolution of better than 500 meV. X-ray absorption was measured in partial electron yield (PEY) detection mode with a retarding voltage of −150 V. For energy calibration, the spectra were referenced to a characteristic peak at 285 eV in the photocurrent spectra of a carbon-contaminated gold grid, which were recorded simultaneously with each NEXAFS spectrum. The position of this peak was calibrated independently against the strong π^* resonance of highly oriented pyrollitic graphite (HOPG), which is located at 285.38 eV.[40] Normalization of the raw spectra with respect to the incident photon flux was achieved by division through the NEXAFS spectrum of a clean gold sample. Finally, the spectra were normalized to the absorption step at 325 eV, a standard procedure described in detail elsewhere.[30] The polarization of the synchrotron beam is better than 90%. For the low anisotropies encountered in this work, the imperfect polarization has only a negligible effect. Angle calibration was done by orienting the same surface exactly parallel to the bright zero-order incident beam yielding an overall accuracy of better than 1°. The escape depth of the secondary electron amounts to about 2 nm[41] and exhibits a weak dependence on the angle between the surface normal and photon angle of incidence.

Results

NEXAFS. A typical NEXAFS spectrum of PMDA−ODA polyimide is displayed in Figure 4. The different resonances are labeled by integer numbers. They originate from transitions of C1s electrons into unoccupied molecular orbitals. The precise assignments are provided in Table 1. The feature at 285 eV consists of two resonances separated by 0.7 eV, which correspond to transitions into the lowest unoccupied π^* orbitals of the PMDA and ODA subunits, respectively. The transition dipole moments of these resonances are oriented perpendicular to the corresponding ring planes.

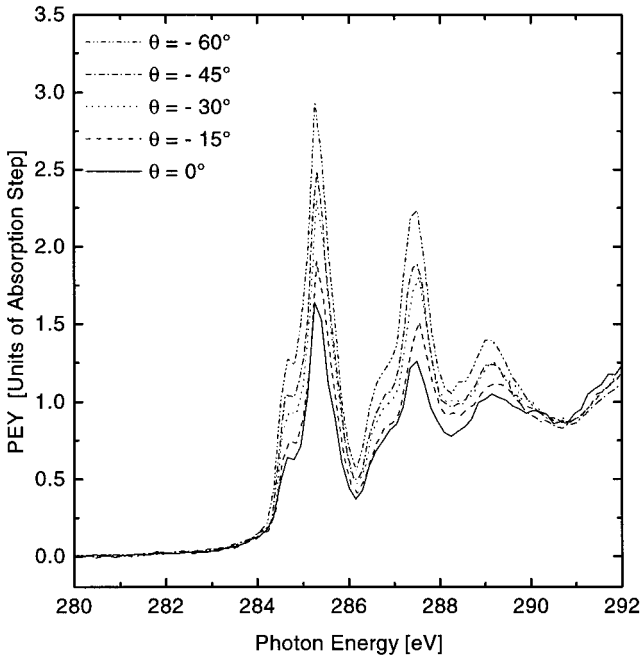

Figure 5. NEXAFS spectra of the strongly buffed sample for different angles of incidence (parallel scan).

Table 1. Assignments of Resonances in the NEXFAS Spectra of PMDA−ODA Polyimide

resonance	energy (eV)	orbital assignments
1	284.6	π^*(C=C) (PMDA)
2	285.3	π^*(C=C) (ODA)
3	286.6	π^*(C=C) (ODA)
4	287.4	π^*(C=O)
5	289.1	π^*(C=C) (ODA)
		π^*(C=C) (PMDA)
6	291.7	σ^*(C=C) (PMDA)
		σ^*(C−O), σ^*(C−N)
7	295.2	σ^*(C=C) (ODA)
8	303.0	σ^*(C=O), σ^*(C=C) (PMDA)
		σ^*(C=C) (ODA)

Figure 5 displays a set of spectra recorded for the strongly buffed sample at the indicated sample orientations. The PMDA and ODA π^* intensities were determined using a fitting procedure. Figure 6 shows the angular variation of resonance intensities as a function of photon angle of incidence for a set of parallel and perpendicular scans together with theoretical curves obtained by fitting the functions $A(\theta) = a_\theta + b_\theta \cos(2(\theta - \theta_0))$ and $A(\varphi) = a_\varphi + b_\varphi \cos(2\varphi)$. From the fit parameters a_θ, b_θ, θ_0, a_φ, and b_φ we can compute S, P, and θ_0; see Table 2. In Table 2 the statistical error bars obtained from the fitting process for S and P are displayed. For the substrate pretilt θ_0 we give the estimated accuracy of angle calibration whenever this is larger than the error from fitting. For the normally buffed sample, the data quality of the perpendicular scans was so low that we discarded the data. We do not quote a value on the biaxiality P. The value for S was derived by assuming that the parameter $\beta = b_\varphi/a_\varphi$ was similar to the other samples and using a much larger error bar for β. Because S mainly depends on α and only weakly on β, this procedure will yield a reliable value.

Figure 6a shows perpendicular scans for the untreated sample and for a weakly buffed sample. For an

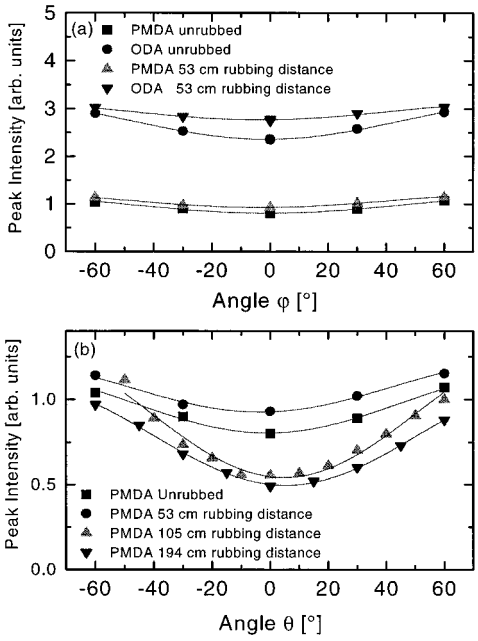

Figure 6. Intensities from the peaks labeled "PMDA" and "ODA" in Figure 4 as a function of sample orientation: (a) perpendicular scans; (b) parallel scans. The straight lines are fits to eqs 5.

Table 2. Order Parameters for the Buffing Strengths and Molecular Units

	S	P	θ_0 (deg)
untreated PMDA	0.122 ± 0.004	0	-1.3 ± 1.0
untreated ODA	0.096 ± 0.002	0	-1.0 ± 1.3
weakly buffed PMDA	0.173 ± 0.005	0.19 ± 0.01	7.8 ± 1.0
weakly buffed ODA	0.116 ± 0.003	0.205 ± 0.01	5.5 ± 1.0
normally buffed PMDA	0.18 ± 0.04		5.0 ± 1.0
normally buffed ODA	0.118 ± 0.02		5.0 ± 1.0
strongly buffed PMDA	0.192 ± 0.002	0.167 ± 0.005	5.2 ± 1.0
strongly buffed ODA	0.158 ± 0.003	0.197 ± 0.006	3.0 ± 1.0

untreated sample there is no distinction between parallel and perpendicular scans due to the in-plane isotropy. During fitting the data from Figure 6a we allowed for an offset φ_0 on the φ scale to check for consistency. In all cases φ_0 was smaller than 1.5°, and $\varphi_0 = 0$ was used in the further analysis of the data. Figure 6a clearly reveals a surface-induced anisotropy for untreated samples. The order parameter S is 0.122 ± 0.004 and 0.096 ± 0.002 for the PMDA units and the ODA units, respectively. The aromatic rings are preferentially aligned with their ring planes parallel to the surface with the absolute amount of alignment being slightly stronger for PMDA than for ODA. We consistently find S larger for the PMDA units than for the ODA units also after buffing. The ODA rings are adjacent to the ether bonds, which are the only flexible joint in the structure, while the PMDA units are situated in the middle of the rigid aromatic block. Presumably, that position is somewhat favorable to parallel alignment along the polymer−air interface.

Anisotropy along the angle φ persists after buffing (Figure 6a). This observation reveals that the buffing-induced chain stretching is not strong enough to lift the surface-induced anisotropy. Again, the anisotropy along the angle φ is stronger for the PMDA units than for the ODA units.

Both the biaxiality P and the inclination θ_0 increase upon buffing (Figure 6b). The inclination θ_0 is of the same order of magnitude as found by IR-birefringence studies.[12] No significant correlations with the buffing strength, however, could be established.

LC Bulk Pretilt Angles. To gather information on the interrelation between the orientational distribution function of the molecular subunits at the polymer surface and that of an LC liquid in contact with such a surface, we have determined the LC pretilt angle using the crystal rotation setup. In this procedure a 30 μm LC cell is rotated between crossed polarizers. From the pattern of transmission maxima and minima the cell thickness and the pretilt angle are derived.[39] The obtained pretilt angles are $2.0 \pm 1°$, $2.3 \pm 1°$, and $2.4 \pm 1°$ for weak, normal, and strong buffing. These values have to be compared to the corresponding substrate pretilt angles of $7.8 \pm 1.0°$, $5.0 \pm 1.0°$, and $5.2 \pm 1.0°$ for the ODA units and $5.5 \pm 0.6°$, $5.0 \pm 1.0°$, and $3.0 \pm 1.0°$ for the PMDA units. Generally speaking, the pretilt of the bulk liquid crystal is smaller than the substrate pretilt. Why the surface pretilt only imperfectly translate into a bulk pretilt remains an open question at this point. Presently, NEXAFS studies on LC monolayers evaporated onto the alignment layers are being carried out to further elucidate this point. Preliminary results seem to indicate that the first monolayer is already less inclined than the substrate.

Neither the bulk liquid LC pretilt nor the substrate pretilt show a strong dependence on buffing strength. Presumably, the effect of buffing saturates at some point in the sense that the induced anisotropy does not increase on further buffing. This observation is in agreement with the work by Samant et al., who report that the buffing-induced anisotropy saturates at a 1/e buffing distance of 67 cm.[29] This buffing distance is slightly higher than the buffing distance of our "weakly" buffed sample.

Quantitatively, the buffing-induced anisotropy is quite small. None of the components of the diagonalized Saupe tensor (eq 4) is larger than 0.2. Typical order parameters for liquid crystals, on the other hand, are on the order of $S \sim 0.45-0.7$. This difference in the degree of order may be related to the difference between substrate pretilt and bulk LC pretilt. Interestingly, the order parameters of liquid crystal monolayers on polyimide surfaces as determined with optical SHG also turned out to be significantly smaller than typical bulk order parameters.[16]

Discussion

An important goal of the analysis of molecular orientations at the buffed PI surfaces is to derive a molecular model consistent with the orientational distribution functions for the different molecular subunits, as determined above. Although a full structural analysis is not possible on the basis of the present data, we can hypothesize about the molecular conformation of the polymer chains at the surface. An inclination of molecular units with respect to the sample surface has previously been observed for other polyimides by Ouchi and co-workers.[27,28] The authors rationalized their findings by assuming that the aromatic cores are assembled at the surface like shingles. This picture implicitly invokes the concept of a "quasi-epitaxial" interaction, where the aromatic cores of the liquid crystal molecules line up with the aromatic cores of the polyimide. The molecular conformation is such that the aromatic cores are tilted with respect to the surface. A shinglelike arrangement along the main chain, however,

requires that the aromatic units are not rigidly linked to each other but rather contain flexible units that can form a double kink. PMDA−ODA, on the other hand, has only one flexible joint between two aromatic blocks. A shinglelike arangement is only plausible between aromatic blocks of different chains. In this case, the explanation would rest on packing of microcrystals, rather than on the conformation of individual chains. One may be able to detect this tilted packing with grazing incidence X-ray scattering.[36,37] Alternatively, the origin of tilt in orientation may be a tilted arrangement of larger clusters comprising many units cells. This should lead to some surface roughness. Scanning force microscope (SFM) studies on rubbed polyimides have indeed shown that the surfaces display a fairly rich structure on different scales.[42] We have taken pictures of the surface investigated here and found that they very much resemble the features termed "nanoislands" in ref 42. The islands are slightly extended into the buffing direction and have a height of some nanometers. Whether the origin of tilt is to be found in a shinglelike arrangement on the molecular level or rather in a tilt of larger clusters remains an open question.

Conclusions and Outlook

We have used X-ray absorption spectroscopy, NEXAFS, to determine the orientational distribution functions of the PMDA and ODA subunits on surfaces of PMDA−ODA polyimide surfaces, which were buffed with different strengths. Untreated samples were found to exhibit uniaxial surface-induced order with an order parameter of $S \approx 0.1$. Upon buffing, biaxiality and an inclination of the principal directions of anisotropy with respect to the sample surface develop. Biaxiality and inclination are only weakly correlated to buffing strength in the investigated range. The bulk pretilt angles measured for liquid crystals in contact with the alignment layers are smaller by a factor of 2−3 than the angles of inclination of the polyimide chains.

In future experiments we will use the same technique employed here, NEXAFS, to study the orientational distribution function of LC layers, which are evaporated in situ onto the alignment layers. We expect that a correlation of these findings with the corresponding data for the polymer surface will allow for more detailed conclusions on the microscopic alignment process.

Acknowledgment. We acknowledge stimulating and helpful discussions with Yukio Ouchi. Also, we thank Martin Baumgarten for help concerning the structure of PMDA−ODA polyimide.

Appendix: Derivation of Order Parameters from the Trigonometric Fit Functions

In the following we provide a detailed derivation of eq 7. The X-ray absorption for a given polarization is given by (eqs 1 and 2)

$$A(\hat{p}) = 3\bar{A}\hat{p}\cdot\vec{\vec{K}}\cdot\hat{p} = 3\bar{A}\hat{p}\cdot\left(\frac{2\vec{\vec{Q}} + \vec{\vec{I}}}{3}\right)\cdot\hat{p} \quad \text{(A1)}$$

or

$$\frac{A(\hat{p})}{\bar{A}} = 2\hat{p}\cdot\vec{\vec{Q}}\cdot\hat{p} + 1 \quad \text{(A2)}$$

In the laboratory frame, the Saupe-matrix $\vec{\vec{Q}}$ is given by

$$\begin{aligned}\vec{\vec{Q}} &= RQ_{\mathrm{dia}}R^{-1}\\ &= \begin{bmatrix}\cos(\theta_0) & 0 & -\sin(\theta_0)\\ 0 & 1 & 0\\ \sin(\theta_0) & 0 & \cos(\theta_0)\end{bmatrix}\begin{bmatrix}-(S+P)/2 & 0 & 0\\ 0 & -(S-P)/2 & 0\\ 0 & 0 & S\end{bmatrix}\begin{bmatrix}\cos(\theta_0) & 0 & \sin(\theta_0)\\ 0 & 1 & 0\\ -\sin(\theta_0) & 0 & \cos(\theta_0)\end{bmatrix}\\ &= \frac{1}{2}\begin{bmatrix}-(P+S)\cos^2\theta_0 + 2S\sin^2\theta_0 & 0 & -1/2(P+3S)\sin(2\pi_0)\\ 0 & -(S-P) & 0\\ -1/2(P+3S)\sin(2\theta_0) & 0 & 2S\cos^2\theta_0 - (P+S)\sin^2\theta_0\end{bmatrix}\\ &= \frac{1}{4}\begin{bmatrix}-P+S-(P+3S)\cos(2\theta_0) & 0 & -(P+3S)\sin(2\theta_0)\\ 0 & -2(S-P) & 0\\ -(P+3S)\sin(2\theta_0) & 0 & -P+S+(P+3S)\cos(2\theta_0)\end{bmatrix}\end{aligned} \quad \text{(A3)}$$

For the parallel and the perpendicular scan (Figure 2a), the polarization vectors $\hat{p}$ are given by

$$\vec{p}_{\parallel} = \begin{bmatrix}\cos\theta\\ 0\\ \sin\theta\end{bmatrix} \quad \text{(A4a)}$$

and

$$\vec{p}_{\perp} = \begin{bmatrix}0\\ \cos\varphi\\ \sin\varphi\end{bmatrix} \quad \text{(A4b)}$$

Insertion of eqs A3 and A4 into eq A2 yields

$$\frac{A(\theta)}{\bar{A}} = \frac{2+S-P}{2} - \frac{P+3S}{2}\cos(2(\theta-\theta_0)) \quad \text{(A5a)}$$

$$\frac{A(\varphi)}{\bar{A}} = \frac{4-S+P+(P+3S)\cos(2\theta_0)}{4} + \frac{3(P-S)-(P+3S)\cos(2\theta_0)}{4}\cos(2\varphi) \quad \text{(A5b)}$$

for the parallel and the perpendicular scans, respectively. We fit the functions $A(\theta) = a_\theta + b_\theta\cos(2(\theta - \theta_0))$ and $A(\varphi) = a_\varphi + b_\varphi\cos(2\varphi)$ to the experimentally determined NEXAFS intensities. The parameters b_0 and a_0 are connected to P and S by

$$\frac{b_\theta}{a_\theta} = \frac{P+3S}{P-S-2} \quad \text{(A6a)}$$

$$\frac{b_\varphi}{a_\varphi} = \frac{3(P-S)-(P+3S)\cos(2\theta_0)}{4+P-S+(P+3S)\cos(2\theta_0)} \quad \text{(A6b)}$$

Eliminating P from eqs A6a and A6b results in

$$\frac{3S+\alpha(S+2)}{\alpha-1} = \frac{\beta(S-4)-3S-3(1+\beta)S\cos(2\theta_0)}{\beta-3+(1+\beta)\cos(2\theta_0)} \quad \text{(A7a)}$$

Eliminating S from eqs A6a and A6b results in

$$\frac{\alpha(P-2)-P}{\alpha+3} = \frac{\beta(P+4)-3P+(1+\beta)P\cos(2\theta_0)}{3-\beta+3(1+\beta)\cos(2\theta_0)} \quad \text{(A7b)}$$

Solving eqs A7a and A7b for S and P yields

$$S = -\frac{1}{2}\frac{3\alpha(\beta-1) - 2\beta + \alpha(\beta+1)\cos(2\theta_0)}{\beta - 3 + \alpha(\beta+1)\cos(2\theta_0)} \quad \text{(A8a)}$$

$$P = \frac{3}{2}\frac{-\alpha(\beta-1) - 2\beta + \alpha(\beta+1)\cos(2\theta_0)}{\beta - 3 + \alpha(\beta+1)\cos(2\theta_0)} \quad \text{(A8b)}$$

These are identical to eqs 7a and 7b in the text.

References and Notes

(1) Jérôme, B. *Rep. Prog. Phys.* **1991,** *54*, 391.
(2) Yokoyama, H. *Mol. Cryst. Liq. Cryst.* **1988**, *165*, 265.
(3) Faetti, S. In *Physics of Liquid Crystalline Materials*; Khoo, J. C., Simoni, F., Eds.; Gordon and Breach: Amsterdam, 1991; Chapter XII.
(4) Uchida, T.; Seki, H. In *Liquid Crystals and Uses*; Bahadur, B., Ed.; World Scientific: Singapore, 1990; Vol. 3, Chapter 5.
(5) Bahadur, B., Ed. *Liquid Crystals and Uses*; World Scientific: Singapore, 1990.
(6) Cognard, J. *Alignment of Liquid Crystals and their Mixtures*; Gordon and Breach: London, 1982.
(7) Myrvold, B. O. *Liq. Cryst.* **1991**, *10*, 771.
(8) Schadt, M.; Seiberle, H.; Schuster A. *Nature* **1996**, *381*, 212.
(9) Shannon, P. J.; Gibbons, W. M.; Sun, S. T. *Nature* **1994**, *368*, 532.
(10) Seki, T.; Sakuragi, M.; Kawanishi, Y.; Suzuki, Y.; Tamaki, T.; Fukuda, R.; Ichimura, K. *Langmuir* **1993**, *9*, 9211 and references therein.
(11) Geary, J. M.; Goodby, J. W.; Kmetz, A. R.; Patel, J. S. *J. Appl. Phys.* **1987**, *62*, 4100.
(12) Sakamoto, K.; Arafune, R.; Ushioda, S.; Suzuki, Y.; Morokawa, S. *J. Appl. Phys.* **1996**, *80*, 431.
(13) Yokokura, H.; Oh-E, M.; Kondo, K.; Oh-hara, S. *Mol. Cryst. Liq. Cryst.* **1990**, *225*, 253.
(14) Toney, M. F.; Russell, T. P.; Logan, J. A.; Kiguchi, H.; Sands, J. M.; Kumar, S. K. *Nature* **1995**, *374*, 709.
(15) Feller, M. B.; Chen, W.; Shen, Y. R. *Phys. Rev. A* **1991**, *43*, 6778.
(16) Johannsmann, D.; Zhou, H.; Sonderkaer, P.; Wierenga, H.; Myrvold, B. O.; Shen, Y. R. *Phys. Rev. E* **1993**, *48*, 1889.
(17) Zhuang, X. W.; Marrucci, L.; Johannsmann, D.; Shen, Y. R. *Mol. Cryst. Liq. Cryst.* **1995**, *262*, 1323.
(18) Zhuang, X. W.; Marrucci, L.; Shen, Y. R. *Phys. Rev. Lett.* **1994**, *73*, 1513.
(19) Barmentlo, M.; Hollering, R. W. J.; van Aerle, N. A. J. M. *Phys. Rev. A* **1992**, *46*, R4490.
(20) Wesch, A.; Dannenberger, O.; Wöll, Ch.; Wolff, J. J.; Buck, M. *Langmuir* **1996**, *12*, 5530.
(21) Himmel, H.; Kaschke, M.; Harder, P.; Wöll, Ch. *Thin Solid Films* **1996**, *284−285*, 275.
(22) Schertel, A.; Hähner, G.; Grunze, M.; Wöll, Ch. *J. Vac. Sci. Technol. A* **1996**, *14*, 1801.
(23) Bierbaum, K.; Hähner, G.; Heid, S.; Kinzler, M.; Wöll, Ch.; Effenberger, F.; Grunze, M. *Langmuir* **1995**, *11*, 512.
(24) Lippitz, A.; Friedrich, J. F.; Unger, W. E. S.; Schertel, A.; Wöll, Ch. *Polymer* **1996**, *37*, 3151.
(25) Lippitz, A.; Koprinarov, I.; Friedrich, J. F.; Unger, W. E. S.; Weiss, K.; Wöll, Ch. *Polymer* **1996**, *37*, 3157.
(26) Jackson, J. D. *Classical Electrodynamics*, 2nd ed.; Wiley: New York 1975.
(27) Ouchi, Y.; Mori, I.; Sei, M.; Ito, E.; Araki, T.; Ishii, H.; Seki, K.; Kondo, K. *Physica B* **1995**, *208* & *209*, 407.
(28) Mori, I.; Araki, T.; Ishii, H.; Ouchi, Y.; Seki, K.; Kondo, K. *J. Electron Spectrosc. Relat. Phenom.* **1996**, *78*, 371.
(29) Samant, M. G.; Stöhr, J.; Brown, H. R.; Russel, T. P.; Sands, J. M.; Kumar, S. K. *Macromolecules* **1996**, *29*, 8334.
(30) Stöhr, J. *NEXAFS Spectroscopy*, Springer Series in Surface Science 25; Springer: Berlin, 1992.
(31) Michl, J.; Thulstrup, E. W. *Spectroscopy with Polarized Light*; VCH Publishers: New York, 1986.
(32) de Gennes, P. G.; Prost, J. *The Physics of Liquid Crystals*; Oxford University Press: Oxford, U.K., 1993.
(33) Bessonov, M. I.; Koton, M. M.; Kudryavtsev, V. V.; Laius, L. A. *Polyimides, Thermally Stable Polymers*; Consultants Bureau: New York, 1987.
(34) Kazaryn, L. G.; Tavankin, D. Ya.; Ginsburg, B. M.; Tuichev, Sh.; Korzhavin, L. N.; Frenkel, S. Ya. *Vysokomol Soed. A* **1972**, *14*, 1199 (*Polym. Sci. USSR* **1972**, *14*, 1344).
(35) Takahashi, N.; Yoon, D. Y.; Parrish, W. *Macromolecules* **1984**, *17*, 2583.
(36) Factor, B. J.; Russell, T. P.; Toney, M. F. *Phys. Rev. Lett.* **1993**, *66*, 1181.
(37) Factor, B. J.; Russell, T. P.; Toney, M. F. *Macromolecules* **1993**, *26*, 2847.
(38) Baur, G.; Wittwer, V.; Berreman, D. W. *Phys. Lett.* **1976**, *56A*, 142.
(39) Scheffer, T. J.; Nehring, J. *J. Appl. Phys.* **1977**, *48*, 1783.
(40) Batson, P. E. *Phys. Rev. B* **1993**, *48*, 2608.
(41) Hähner, G.; Kinzler, M.; Thümmler, C.; Wöll, Ch.; Grunze, M. *J. Vac. Sci. Technol. A* **1992**, *10*, 2758.
(42) Pidduck, A. J.; Bryan-Brown, G. P.; Haslam, S.; Bannister, R.; Kitely, I.; McMaster, T. J.; Boogaard, L. *J. Vac. Sci. Technol. A* **1996**, *14*, 1723.

MA971075Z